Journal of MATERIALS RESEARCH

Article
DOI: 10.1557/jmr.2019.43

Research on the coarsening mechanism of precipitations and its effect on toughness for nickel-based weld metal during thermal aging

Tongjiao Chu[1], Huali Xu[1], Haichao Cui[1], Fenggui Lu[1,a)]

[1]Shanghai Key Laboratory of Materials Laser Processing and Modification, School of Materials Science and Engineering, Shanghai Jiao Tong University, Shanghai 200240, People's Republic of China

[a)]Address all correspondence to this author. e-mail: Lfg119@sjtu.edu.cn

Received: 14 December 2018; accepted: 22 January 2019

Coarsening mechanism of precipitations was investigated in a weld metal of Alloy 617 during long-term aging at 750 °C, and its effect on impact toughness was clarified distinctly. The needle-like M_6C phases at the grain boundary nucleated and coarsened at 2000 h and then presented a stable size with aging to 8000 h. Spherical γ′ phase grew rapidly with the rate of 0.0121 nm/h when aged at 1000 h; then, its ripening rate (RR) reduced to 0.0033 nm/h at 8000 h and stabilized around it. The coarsening of M_6C and γ′ was, respectively, controlled by interface diffusion and volume diffusion with the coarsening rate constant of 7.865×10^{-20} m^2/s and 1.519×10^{-27} m^3/s. Interaction of M_6C and γ′ could facilitate their coarsening and cause dramatic decrease in toughness at the early stage. At aging to 8000 h and more, the lower RR of needle-like M_6C phases and γ′ phases helped to form stable toughness at a later stage.

Introduction

Nickel-based alloy has been preferentially selected to use in aerospace, power industry, etc., for its high strength and better resistance to corrosion and oxide at elevated temperatures [1, 2]. As one of nickel-based alloys, Alloy 617 is mainly composed by Ni–Cr–Co–Mo, which is expected to serve at elevated temperatures [2]. Thus, the mechanical behavior of Alloy 617 at high temperatures is significantly important, which is mainly influenced by phase precipitations.

As a kind of alloy with solid-solution strengthening and aging strengthening, the nickel-based alloy contains various types of precipitations. Cozar et al. [3] reported the nanoscaled γ′-Ni_3Al (cubic or spherical shape) and γ″-Ni_3Nb precipitations (lens-like disk shape) in Inconel 718. $M_{23}C_6$ could lose Cr atoms and form M_6C as follows: $M_{23}C_6 + Mo \rightarrow M_6C$ [4, 5]. Yang et al. [6] reported that M (metal atoms) directly reacted with C (carbon) as follows: $6M + C \rightarrow M_6C$. These precipitations would coarsen during long-term thermal exposure, which was controlled by coarsening kinetics [7, 8]. Li et al. [9] described the coarsening process of Ni_3Al and Ni_3V in $Ni_{75}Al_xV_{25-x}$ alloys through Langer and Schwartz model obtained from Ostwald ripening theory. The coarsening behavior of γ′ phases was in accordance with matrix diffusion and had very low interfacial energies [10]. Wu et al. [11] suggested that the coarsening of γ′ phases followed the cube rate law at the early stage and the square rate law at the later stage. However, only limited information is available in general describing and qualitatively determining the coarsening behavior of γ′ phases [12, 13], and the coarsening mechanism needs to be refined to each growth process. Compared with γ′ phases, the coarsening mechanism of M_6C phases was studied insufficiently. Additionally, there are few detailed reports about the effect of coarsening mechanism on toughness.

The precipitation evolution would play a significant role during long-term exposure at high temperatures in Ni-based alloy [14, 15]. Wu et al. [16] interpreted the increase in strengthening by precipitation hardening or coherency strain hardening mechanism of γ′ phase [17, 18, 19], which could increase the risk of dropping in toughness. A large drop in microhardness has been obtained due to a substantial decrease in the volume fraction of γ′ phase and coarsening of the carbides with long-term exposure at 871 °C [16]. Besides γ′ phase, some carbide precipitating at the grain boundary (GB) could influence the mechanical performance, such as the

Cr-enriched $M_{23}C_6$ and the Mo-enriched M_6C. Liu et al. [20] reported that M_6C carbide in Ni-based single crystal superalloy was beneficial to the long-term creep properties at 1038 °C. M_6C phase is prevalent with the needle-like shape and has coherent relationship with the matrix [21]. The carbide at GB inhibits dislocation motion and pins dislocation, then leads to stress concentration, and promotes the formation of microcracks [22]. There exist a lot of researches on the characterization of individual precipitation, while few researches focus on the interaction role of various precipitations. Moreover, the toughness could be influenced by the interaction role of precipitations, which deserves to be studied in detail.

Based on the aforementioned key points, the purpose of this study was to investigate the coarsening mechanism of precipitations during long-term aging at an elevated temperature of 750 °C and to further explore its effect on impact toughness of the nickel-based weld metal (WM). In the present study, a series of exposure times were performed on the WMs, and the corresponding aging specimens were used to measure the impact toughness. The microstructure of different aging times in the WM was characterized by scanning electron microscopy (SEM) and scanning transmission electron microscopy (STEM). With the experimental results and analysis of the thermal exposure, the evolution behavior of Mo-enriched M_6C and γ' phases and their effect on toughness were elaborately discussed. The growth rate of precipitations with time and stable toughness will be predicted based on the analysis, which will help in guiding the design on service life.

Results and discussion

Impact analysis

Toughness is an important mechanical property that could reflect internal defects in the material and the resistance to localized plastic deformation and is sensitive to long-term thermal aging. Figure 1 presented the impact toughness result of WMs under different aging times. The toughness had fallen to 65% when aging time up to 2000 h with a rapid speed and then declined slowly to 51% at 8000 h. From 8000 to 12,000 h, the toughness of the WM decreased slightly to 48.4 J, which indicated that the evolution of the WM gradually tended to be stable. Intergranular and transgranular mode appeared on the fracture morphology, as shown in Figs. 1(a) and 1(b). Thus, the variation tendency of impact toughness could be ascribed to the precipitations and their evolution both in the grain and at GB.

Microstructure of the WM without thermal aging

To better understand the changes in toughness, it is necessary to characterize the microstructure of the WM without thermal aging (shown in Fig. 2 and Table I). The WM was mainly a columnar grain that was bounded by grain boundaries. The precipitations distributed in the WM were owing to the process of post-weld heat treatment (PWHT). Different bright and dark contrasts in the backscattered electron (BSE) image presented different precipitations: the gray contrast at GB, the bright contrast, and the black contrast in the grain. Assisted by the energy-dispersive X-ray spectrometer (EDS) results in Table I, it could be identified that the gray contrast at GB was Cr-enriched phases, the bright contrast in the grain was Mo-enriched phases, and the black contrast was Ti(C, N). Besides, the Mo-enriched phases were M_6C phases according to researches [23, 24] and could be determined in the following analysis. The spherical precipitation [shown in Fig. 2(d)] characterized with size less than 10 nm would be identified to be γ' phases in the following analysis.

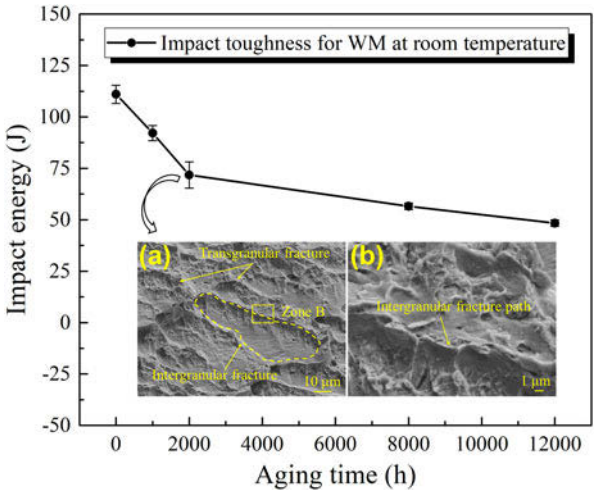

Figure 1: The variation of impact toughness with aging times at 750 °C. 2000 h: (a) the impact fracture; (b) magnification of zone B shown in (a).

TABLE I: EDS results (wt%) of the precipitations shown in Figs. 2(a) and 2(b).

Elements	Cr	Mo	C	Al	Co	N	Ti	Ni
Point A	**57.26**	19.62	2.85	0.40	4.39	1.10	0.13	14.26
Point B	21.48	**45.17**	3.22	0.48	6.09	2.03	0.77	20.77
Point C	28.00	9.14	1.81	0.53	4.26	**15.53**	**22.05**	18.69

Characterization of microstructure evolution

Figure 3 displayed the characteristics of precipitations at GB after long-term aging. To clearly observe the precipitations, BSE images in inset were used to magnify the detailed morphology. Similar to the WM without aging, the precipitations at GB were mainly Cr-enriched phases when aged to 1000 h, as shown in Fig. 3(a). As aging time increased to 2000 h, the needle-like Mo-enriched phases began to form at GBs. Then,

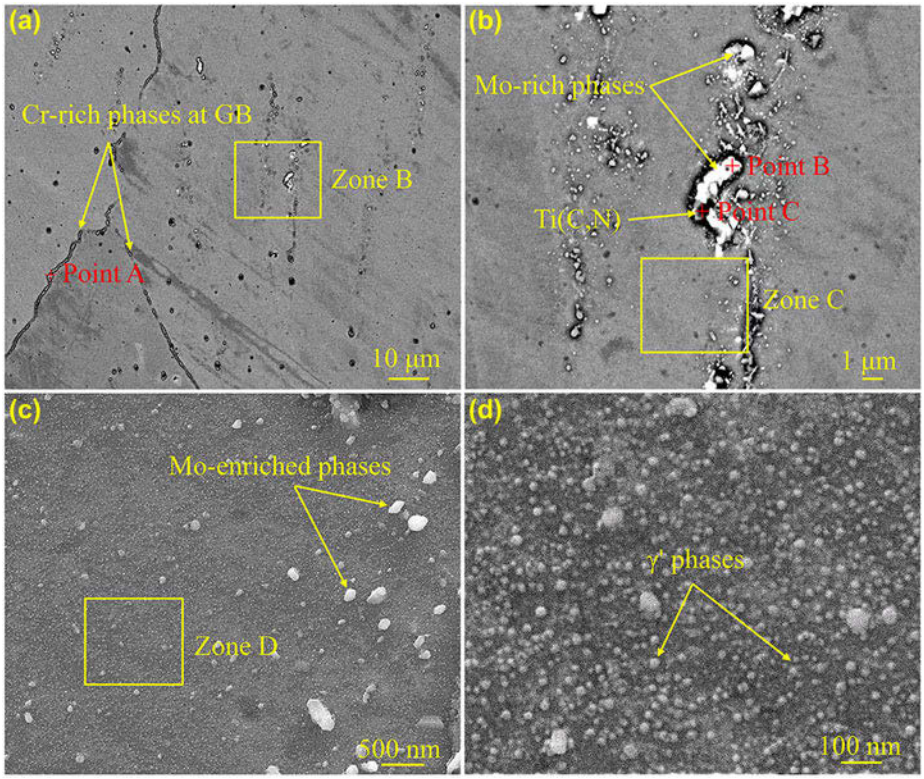

Figure 2: Microstructure of the WM without aging process: (a) BSE image of the WM; (b) magnification of zone B in (a); (c) morphology of γ′ phases; (d) magnification of zone D in (c).

the Mo-enriched phases evolved to the certain needle-like shape at the time of 8000 h, which had an orientation relationship with the matrix and could cause stress concentration. Although the WM experienced such a long-term exposure from 8000 to 12,000 h, the Mo-enriched phases could keep the needle-like shape and similar size present in the stable state. These needle-like Mo-enriched precipitations in GB behaved hard and brittle, which were easy to produce microcracks and had great tendency to promote further fractures.

Besides, at GB, some Mo-enriched phase could also be observed in the grain, as shown in Fig. 4. Different from the needle-like shape at GB, the Mo-enriched phases in the grain presented to be rod-like. When aged for 1000 h, the rod-like Mo-enriched phases were nearly 600 nm in length. As aging time increased to 8000 h, the rod-like Mo-enriched phases had little growth in length, occurring with mild extension in width. The rod-like Mo-enriched phases were relatively stable during long-term thermal aging; thus, it would have little effect on the mechanical property.

As mentioned above, there existed a lot of tiny γ′ phases in the grain. With the aging time increasing, the size of spherical γ′ phases varied greatly as shown in Fig. 5. At the aging time of 1000 h, the size of γ′ phases grew up to 60 nm in radius with dispersed distribution, and most of these γ′ phases were individual. The aggregation and coarsening of γ′ phases were found with the reduction in number at 2000 h, which could be used to explain the growth of γ′ phases. The number of γ′ phases decreased greatly at 8000 h; meanwhile, the mean size could reach around 130 nm due to the aggregation and coarsening. No obvious change in the number and size of γ′ phases was found at the aging time of 12,000 h. The γ′ phases grew at the expense of their number and would arrive at a stable state in WMs with an extension in the aging time. The size of γ′ phases played an important role in the mechanical property. According to researches [25, 26], the γ′ phases as deformable particles could be easily cut by dislocation. As the γ′ phases increase, cutting process could become harder, and the hardness of WM was enhanced. The higher hardness in the WM promoted the easy fracture of the WM and presented a lower toughness.

Quantitative analysis of microstructure evolution

To clearly demonstrate the microstructure evolution, quantitative analysis for precipitations was performed. Needle-like Mo-enriched phases at GB began to form the length of 1.19 μm at 2000 h and obviously grew to 1.76 μm at 8000 h; then their length increased mildly when aged to 12,000 h. Different from Mo-enriched phases at GB, the rod-like Mo-enriched phases in the grain had a small size and coarsened slightly during long-term thermal aging, as shown in Fig. 6(b). The coarsening

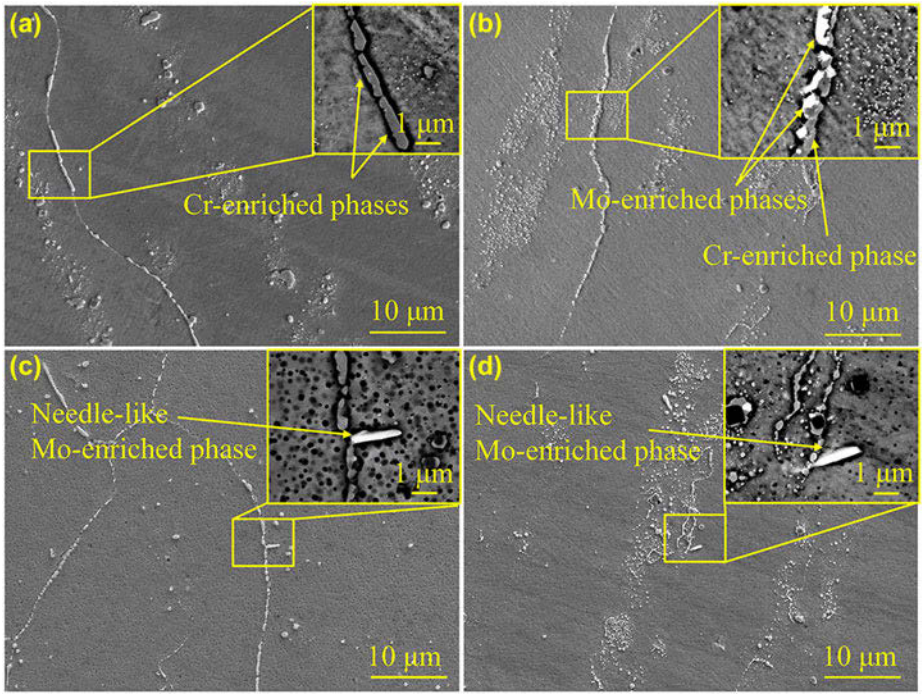

Figure 3: Microstructure of Mo-enriched phases in the WM experiencing thermal aging with various times: (a) 1000 h; (b) 2000 h; (c) 8000 h; (d) 12,000 h.

process of γ′ phases had the similar tendency with needle-like Mo-enriched phases, as shown in Figs. 6(c) and 6(d). Due to the process of PWHT, there existed the size of 26.54 nm for γ′ phases in WMs without thermal aging, and then γ′ phases obviously grew up to 131 nm from 1000 to 8000 h. Continuing thermal aging, γ′ phases coarsened hardly to 140 nm when aged to 12,000 h, and their area fraction also changed slowly.

Ostwald ripening theory could explain this coarsening process for precipitations, and the quantitative description of the ripening in the two-phase system was given by the Lifshitz–Slyozov theory [27]. The size of precipitations follows a power-law of the form:

$$d = k \cdot t^{\alpha} + a \quad , \tag{1}$$

where d is the size of precipitations, t is the aging time, a is a constant value related to the original size, and α is the growth exponent. Meanwhile, α characterizes the underlying dynamics typically for the observed coarsening mechanism, where $\alpha = 1/3$ for volume diffusion-controlled Ostwald ripening and $\alpha = 1/2$ for interface-controlled Ostwald ripening and curvature-driven growth [28]. According to the Ostwald theory, fitting curves were processed in Figs. 6(a) and 6(c), and the fitted results were shown as follows:

$$M_6C \text{ phases} : L = 0.01 \times t^{0.56369},\ R^2 = 0.79865 \quad , \tag{2}$$

$$\gamma' \text{ phases} : r = 11.35 \times t^{0.2695},\ R^2 = 0.99365 \quad , \tag{3}$$

where L is the length of M_6C phases and r is the mean diameter of γ′ phases. Eqs. (2) and (3), respectively, figured out that the coarsening process for M_6C phases and γ′ phases agreed with the growth exponent of 1/2 and 1/3, respectively, indicating that the growth of M_6C phases and γ′ phases was of different mechanisms. The coarsening of M_6C phase was in accordance with the growth exponent of 1/2 and controlled by interface diffusion, which could also be judged from its needle-like shape and its inhomogeneous distribution in matrix. However, the spherical shape of γ′ phase and its homogeneous distribution in the matrix revealed the volume diffusion mechanism, which agreed with the growth exponent of 1/3.

Interaction of microstructure evolution and its influence on toughness

Various precipitations separately developed their own morphology on the surface, but there existed a remarkable internal relationship in fact. As shown in Figs. 7(a) and 7(b), spherical γ′ phases grew preferentially at the face site of needle-like M_6C phases due to element diffusion during thermal aging. Figure 7(c) shows the microstructure of precipitations in WMs at 8000 h, together with the elemental map analysis in Fig. 7(d) and selected area diffraction (SAD) analyses in Figs. 7(e) and 7(f). It could be determined that this microstructure was composed by M_6C (Mo-enriched phase), $M_{23}C_6$ (Cr-enriched phases), and γ′ phases. The ripening process of γ′ phases was the diffusion of Ni, Al, and Ti from small particles to large particles. During the formation of Mo-enriched phases, non-constituent elements were expelled to its interface with matrix. Thus, the γ′

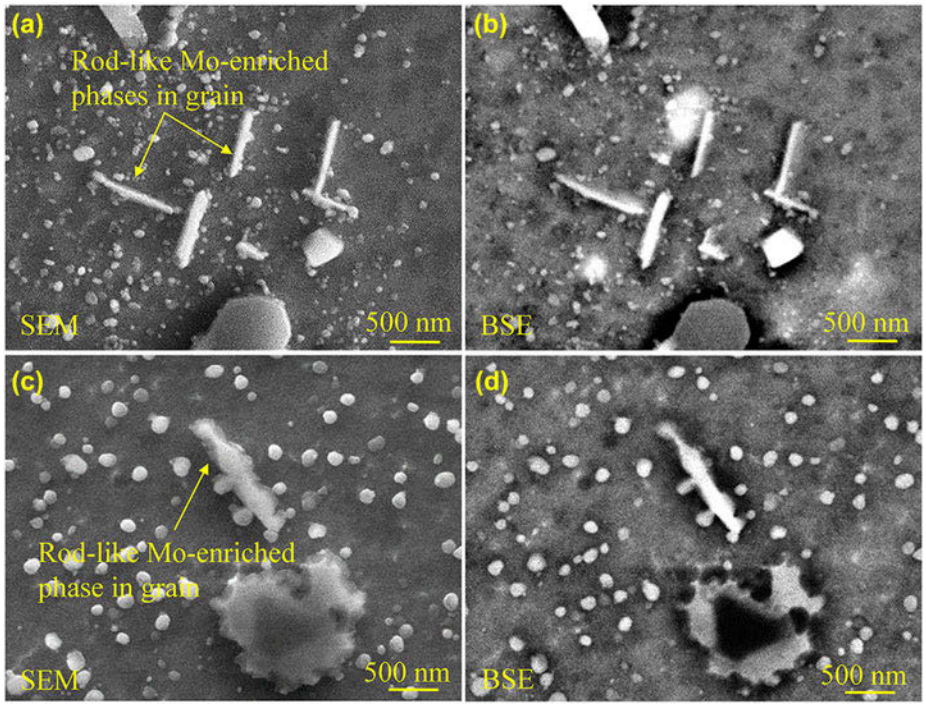

Figure 4: Microstructure of the rod-like Mo-enriched phases in the grain for WM experiencing elevated temperature aging: (a) and (b) 1000 h; (c) and (d) 8000 h. (a) and (c) were SE images, while (b) and (d) were BSE images.

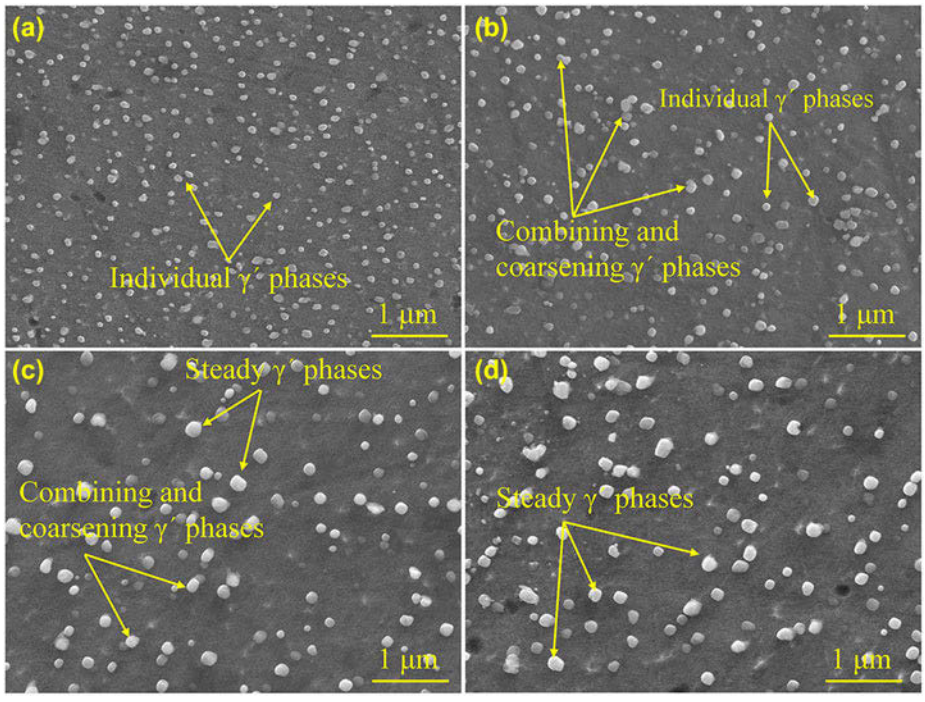

Figure 5: Microstructure of γ′ phases at (a) 1000 h, (b) 2000 h, (c) 8000 h, and (d) 12,000 h.

phases had a great tendency to precipitate at the face site of Mo-enriched phases. Reciprocally, the coarser γ′ phases at the interface of Mo-enriched phase hindered the diffusion of Mo to the direction of Mo-enriched phases, which caused the size of Mo-enriched phases to increase. Thus, the ripening process for γ′ phases restricted the growth of needle-like Mo-enriched phases, and this hindering role was consolidated with the passage of time.

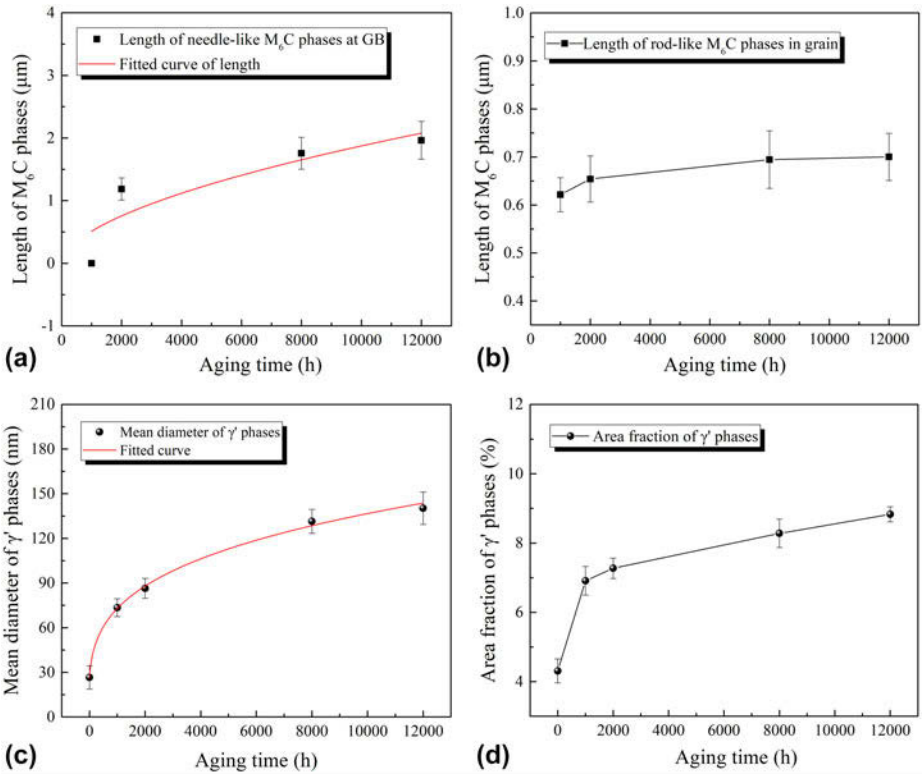

Figure 6: Evolution of precipitations in the WMs thermally aging at 750 °C: (a) length of needle-like M_6C phases at GB; (b) length of rod-like M_6C phases in the grain; (c) mean diameter of γ′ phases; (d) area fraction of γ′ phases.

This interaction during the growth of M_6C phases and γ′ phases could be affected by their coarsening mechanisms. Coarsening rate constant K described coarsening kinetics of precipitations and could be obtained from the following form:

$$K = k^{1/\alpha} \quad . \tag{4}$$

Thus, the coarsening rate constant K of M_6C phases and γ′ phases could be determined from Eqs. (2)–(4), which were 7.865×10^{-20} m^2/s and 1.519×10^{-27} m^3/s, respectively. The coarsening kinetic for M_6C phase was higher than that for γ′ phase, which was ascribed to its preferential growth in interface. To further evaluate the coarsening kinetic of γ′ phases in each growth phase, ripening rate (RR) had been calculated according to the derivation of Eqs. (2) and (3), and the expression of RR for M_6C phases and γ′ phases was shown as follows:

$$M_6C \text{ phases} : \frac{\partial r}{\partial t} = 0.006 \times t^{-0.43631} \quad , \tag{5}$$

$$\gamma' \text{ phases} : \frac{\partial r}{\partial t} = 2.97 \times t^{-0.72406} \quad . \tag{6}$$

The RRs for M_6C phases and γ′ phases at each aging time are shown in Fig. 8. Because the appearance of needle-like M_6C phases at GB was from 2000 h, thus its data of RR at 1000 h was not involved in Fig. 8(a). The RR for M_6C phases decreased obviously at 8000 h, and then it showed a slight change when aged to 12,000 h. It could be found the RR of γ′ phases dropped to a relatively low value when aging time increased to 2000 h, as shown in Fig. 8(b). Continuing aging, the RR of γ′ phases remained low at 8000 and 12,000 h, indicating that a stable state for γ′ phases had been reached. In addition, the longer aging time, 16,000 and 20,000 h, was considered in Eqs. (5) and (6) to predict the RR for M_6C phases and γ′ phases, which could be used to further judge the stable state. Compared with the RR at 8000 h for both precipitations, the predicted RR for longer aging time decreased slowly, which suggested the stable state formed when aged at 8000 h. Thus, both M_6C phases and γ′ phases coarsened drastically at the early aging stage, grew in a mild way, and then could be in a stable state although aging time increased.

This interaction mechanism and coarsening mechanism had a large effect on impact toughness. At first, γ′ phases precipitated in the grain and coarsened obviously as aging time increased. The γ′ phases were cut by dislocations, and the cutting action became harder with the coarser γ′ phases; then, a pileup occurred. These behaviors between γ′ phases and dislocations played a role of coherency strain hardening in WM and caused a reduction in toughness during ripening

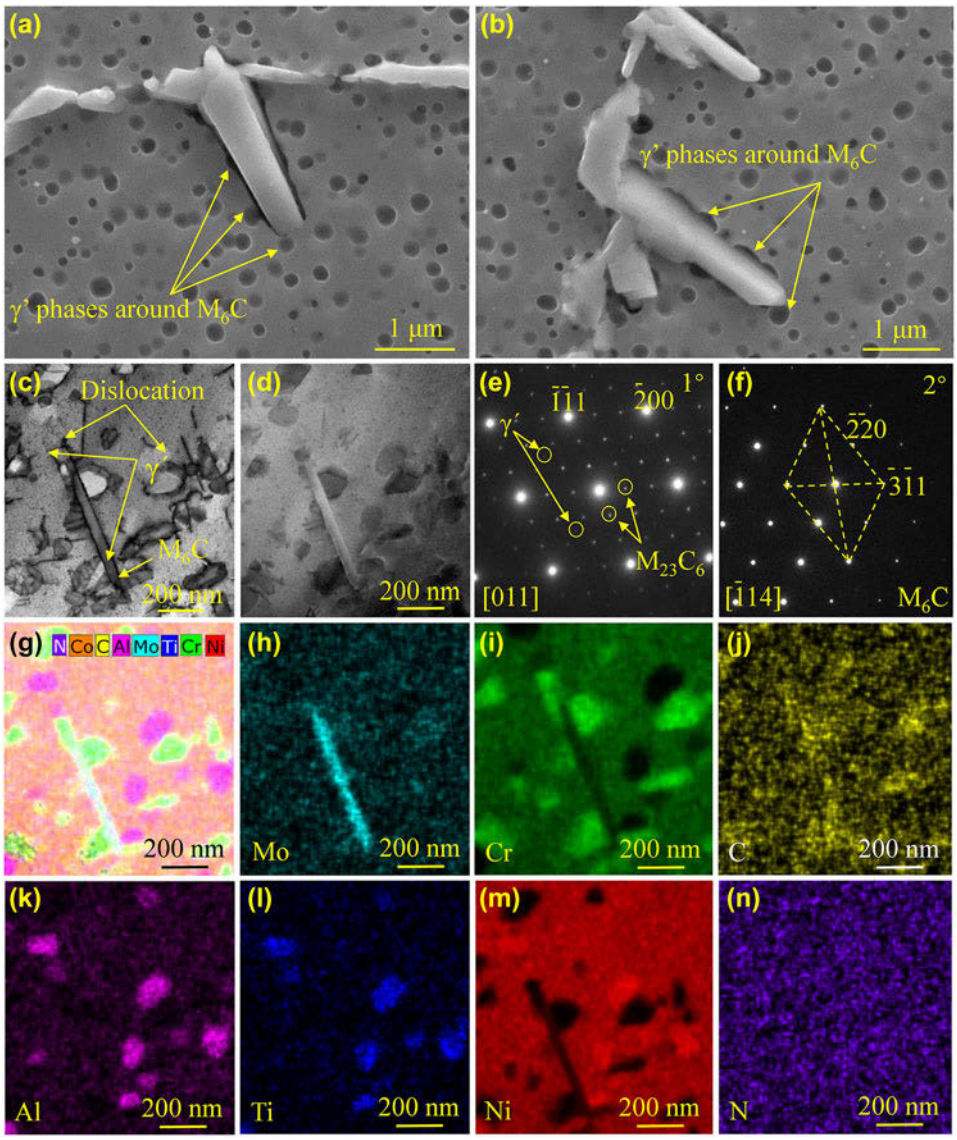

Figure 7: The interaction morphology of the γ′ phases and needle-like Mo-enriched phases aging for (a) 8000 h and (b) 12,000 h. TEM analysis results of the microstructure in the WM aging for 8000 h: (c) bright field image; (d) HADDF image; (e) and (f) SADP of M_6C, $M_{23}C_6$ and γ′ phases; (g) stacking area of the STEM-Map analysis; (h)–(n) the mapping of Mo, Cr, C, Al, Ti, Ni and N.

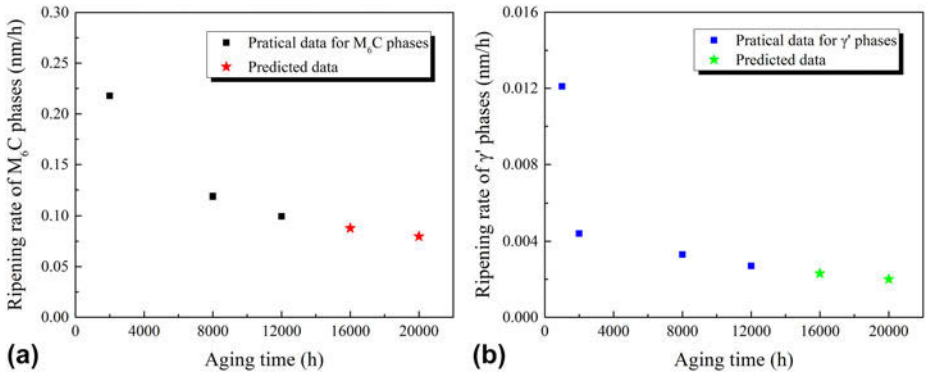

Figure 8: RRs for the precipitations at the tested time and predicted time: (a) M_6C; (b) γ′ phases.

TABLE II: The main chemical compositions (wt%) of BM and FM.

Elements	C	Cr	Mo	Fe	Al	Co	B	Nb	Ti	Ni
BM	0.036	21.63	9.15	0.29	1.02	12.00	0.0057	0.041	0.48	Bal.
FM	0.054	21.93	9.02	0.71	1.27	11.05	0.0055	0.015	0.35	Bal.

process. Simultaneously, the needle-like Mo-enriched phase grew up and caused heavy stress concentration, which could be responsible for the lower toughness. Increasing the aging time, γ′ phases and M_6C phases continued coarsening, but the RR slowed down. Meanwhile, the needle-like shape of Mo-enriched began to be certain and no more deteriorated. Thus, the effect of γ′ phases and the needle-like Mo-enriched phases on toughness became moderate, and a stable state was built for the WM at the later stage of aging.

Conclusions

The microstructure evolution of M_6C phases and γ′ phases in WM of Alloy 617 and its effect on toughness have been systematically investigated at 750 °C, which could provide assistance to practical operations. The obtained results are summarized as follows:

(1) The size of spherical γ′ phases increased as the exposure time prolonged from 1000 to 12,000 h, which was controlled by volume diffusion and adhered to Ostwald ripening theory. In detail, γ′ phases coarsened rapidly at early and then grew slightly when the exposure time increased from 8000 to 12,000 h.

(2) The M_6C phases coarsened in the needle-like shape at GB and rod-like shape in the grain; the latter had a small size and changed hardly during thermal aging. The needle-like M_6C phases at GB began to nucleate and coarsen at 2000 h and then presented a stable size with aging time increasing from 8000 to 12,000 h. Furthermore, the coarsening rate constant of 7.865×10^{-20} m^2/s for needle-like M_6C phases was higher than that for γ′ phases due to its preferential growth being controlled by interface diffusion.

(3) The interaction mechanism between M_6C phases and γ′ phases could promote their coarsening process and cause the dramatic decrease in toughness at the early aging stage. At aging to 8000 h and more, RR of needle-like M_6C phase and γ′ phases gradually reduced, which led to the stable toughness at the later aging stage.

Experimental procedure and materials

The method of narrow gap tungsten inert gas (NG-TIG) welding was selected to produce the single pass and multilayer welded joint of Alloy 617. The chemical compositions of the base metal (BM) and the filler metal (FM) are given in Table II. To relieve the residual stress and get the microstructure stable, the PWHT was performed on all the joints at 980 °C holding for 10 h.

Due to the requirement of practical operation for advanced ultra-supercritical (A-USC) plants, the temperature of 750 °C was chosen to perform the thermal aging process. The WMs of Alloy 617 with multilayers were aged for 1000 h, 2000 h, 8000 h, and 12,000 h, respectively. To evaluate the mechanical property of WMs experiencing long-term aging, impact tests were carried out on the corresponding aging specimens. According to the ASTM E23-96, Charpy impact tests were measured on the specimen with the size of 55 ×10 × 10 mm, and three specimens for each aging time were tested to ensure precision. The notch of Charpy impact specimens was located in the center of the WM and its bottom line was perpendicular to the welding direction.

The WMs with crack growth path were inlaid at first and subsequently electrochemically polished with a voltage of 25 V at room temperature in a mixture of 10% perchloric acid + 90% ethanol. Then, the WMs were etched in a solution of 80% glacial acetic acid and 20% perchloric acid to obtain the clear microstructure with various second phases. To identify the morphology and composition of second phases, the microstructure of WMs was investigated by a scanning electron microscope (SEM) of JEOL JSM-7800F Prime (Tokyo, Japan) with an energy-dispersive X-ray spectrometer (EDS) and backscattered electrons (BSEs) at 15 kV. The sizes and area fractions of the γ′ particles were measured at SE images with the magnification of 20,000. Furthermore, the scanning transmission electron microscopy (STEM; FEI Talos F200X, Waltham, Massachusetts) was employed to characterize the precipitation with the sample prepared by focused ion beam (FIB; *GAIA3 GMU Model 2016/*GAIA3, Brno, Czech Republic).

Acknowledgments

The authors gratefully acknowledge the financial supports by the National Natural Science Foundation of China (Nos. U1660101, 51675336, and 51775338).

References

1. **Z.B. Yang, J. Sun, S. Lu, and L. Vitos**: Assessing elastic property and solid-solution strengthening of binary Ni–Co, Ni–Cr, and

ternary Ni–Co–Cr alloys from first-principles theory. *J. Mater. Res.* **33**, 2763 (2018).

2. **L. Yuan, R. Hu, and J. Li**: Evolution behavior of superlattice phase with Pt_2Mo-type structure in Ni–Cr–Mo alloy with low atomic Mo/Cr ratio. *J. Mater. Res.* **31**, 427 (2016).
3. **R. Cozar and A. Pineau**: Morphology of γ′ and γ″ precipitates and thermal stability of Inconel 718 type alloys. *Metall. Trans.* **4**, 47 (1973).
4. **J. Xie, J. Shen, N. Chen, and S. Seetharaman**: Site preference and mechanical properties of $Cr_{23-x}T_xC_6$ and $Fe_{21}T_2C_6$ (T = Mo, W). *Acta Mater.* **54**, 4653 (2006).
5. **C.T. Sims, N.S. Stoloff, and W.C. Hagel**: *Superalloys II*, 2nd ed. (Wiley-Interscience Press, USA, 1987); pp. 415–420.
6. **F.M. Yang, X.F. Sun, W. Zhang, Y.P. Kang, H.R. Guan, and Z.Q. Hu**: Secondary M_6C precipitation in K40S cobalt-base alloy. *Mater. Lett.* **49**, 160 (2001).
7. **C.S. Wang, Y.A. Guo, J.T. Guo, and L.Z. Zhou**: Gamma prime stability and its influence on tensile behavior of a wrought superalloy with different Fe contents. *J. Mater. Res.* **31**, 1361 (2016).
8. **J. Ribis, E. Bordas, P. Trocellier, Y. Serruys, Y. de Carlan, and A. Legris**: Comparison of the neutron and ion irradiation response of nano-oxides in oxide dispersion strengthened materials. *J. Mater. Res.* **30**, 2210 (2015).
9. **Y.S. Li, Z. Chen, Y.L. Lu, and Y.X. Wang**: Coarsening kinetics of intermetallic precipitates in $Ni_{75}Al_xV_{25-x}$ alloys. *J. Mater. Res.* **22**, 61 (2007).
10. **S. Meher, M.C. Carroll, T.M. Pollock, and L.J. Carroll**: Designing nickel base alloys for microstructural stability through low γ–γ′ interfacial energy and lattice misfit. *Mater. Des.* **140**, 249 (2018).
11. **Y. Wu, Y. Liu, C. Li, X. Xia, J. Wu, and H. Li**: Coarsening behavior of γ′ precipitates in the γ′ + γ area of a Ni_3Al-based alloy. *J. Alloys Compd.* **771**, 526 (2019).
12. **H.J. Zhou, F. Xue, H. Chang, and Q. Feng**: Effect of Mo on microstructural characteristics and coarsening kinetics of γ′ precipitates in Co–Al–W–Ta–Ti alloys. *J. Mater. Sci. Technol.* **34**, 799 (2018).
13. **F. Zhang, W. Cao, C. Zhang, S. Chen, J. Zhu, and D. Lv**: Simulation of Co-precipitation kinetics of γ′ and γ″ in superalloy 718. In *Proceedings of the 9th International Symposium on Superalloy 718 & Derivatives: Energy, Aerospace, and Industrial Applications* E. Ott, X.B. Liu, J. Andersson, Z.N. Bi, K. Bockenstedt, I. Dempster, J. Groh, K. Heck, P. Jablonski, M. Kaplan, D. Nagahama and C. Sudbrack eds.; Springer Publishing: Berlin, Germany, 2018; P.147.
14. **G.E. Fuchs**: Solution heat treatment response of a third generation single crystal Ni-base superalloy. *Mater. Sci. Eng., A* **300**, 52 (2001).
15. **E.O. Ezugwu, Z.M. Wang, and A.R. Machado**: The machinability of nickel-based alloys: A review. *J. Mater. Process. Technol.* **86**, 1 (1999).
16. **Q. Wu, H. Song, R.W. Swindeman, J.P. Shingledecker, and V.K. Vasudevan**: Microstructure of long-term aged IN617 Ni-base superalloy. *Metall. Mater. Trans. A* **39**, 2569 (2008).
17. **X.Z. Zhou and Y.C. Su**: Microstructure of long-term aged IN617 Ni-base superalloy. *Mater. Sci. Eng., A* **527**, 5153 (2010).
18. **E. Donoso, R. Espinoza, M.J. Diánez, and J.M. Criad**: Microcalorimetric study of the annealing hardening mechanism of a Cu–2.8Ni–1.4Si (at.%) alloy. *Mater. Sci. Eng., A* **556**, 612 (2012).
19. **J. Oblak, D. Paulonis, and D. Duvall**: Coherency strengthening in Ni base alloys hardened by DO 22 γ′ precipitates. *Metall. Trans.* **5**, 143 (1974).
20. **L.R. Liu, T. Jin, N.R. Zhao, Z.H. Wang, X.F. Sun, H.R. Guan, and Z.Q. Hu**: Effect of carbon addition on the creep properties in a Ni-based single crystal superalloy. *Mater. Sci. Eng., A* **385**, 105 (2004).
21. **J. Yang, Q. Zheng, X. Sun, H. Guan, and Z. Hu**: Relative stability of carbides and their effects on the properties of K465 superalloy. *Mater. Sci. Eng., A* **429**, 341 (2006).
22. **M.K. Ali, M.S.J. Hashmi, and B.S. Yilbas**: Fatigue properties of the refurbished INCO-617 alloy. *J. Mater. Process. Technol.* **118**, 45 (2001).
23. **O.Y. Jun, R.W. Seog, S. Changmo, K.I. Hiun, and H.J. Hwa**: Grain boundary filmlike Fe–Mo–Cr phase in nitrogen-added type 316l stainless steels. *J. Mater. Res.* **14**, 8 (1999).
24. **L. Lirong, C. Maokai, T. Sugui, Z.Y. Zhang, and J. Tao**: Effect of Re content on precipitation behaviour of secondary phases in a single-crystal Ni-based superalloy during high-temperature thermal exposure. *Mater. High Temp.* **35**, 355 (2018).
25. **K. Yashiro, F. Kurose, Y. Nakashima, K. Kubo, Y. Tomita, and H.M. Zbib**: Discrete dislocation dynamics simulation of cutting of γ′ precipitate and interfacial dislocation network in Ni-based superalloys. *Int. J. Plast.* **22**, 713 (2006).
26. **Y.Q. Sun and P.M. Hazzledine**: A TEM weak-beam study of dislocations in γ′ in a deformed Ni-based superalloy. *Philos. Mag. A* **58**, 603 (1988).
27. **R. Finsy**: On the critical radius in Ostwald ripening. *Langmuir* **20**, 2975 (2004).
28. **P. Streitenberger and D. Zöllner**: The envelope of size distributions in Ostwald ripening and grain growth. *Acta Mater.* **88**, 334 (2015).